NeuroImage 170 (2018) 424–433

Contents lists available at ScienceDirect

NeuroImage

journal homepage: www.elsevier.com/locate/neuroimage

Phase-synchronization-based parcellation of resting state fMRI signals reveals topographically organized clusters in early visual cortex

Nicolás Gravel [a,*], Ben M. Harvey [b,c], Remco J. Renken [d], Serge O. Dumoulin [c], Frans W. Cornelissen [a]

[a] Laboratory of Experimental Ophthalmology, University Medical Center Groningen, University of Groningen, Groningen, The Netherlands
[b] Experimental Psychology, Helmholtz Institute, Utrecht University, Utrecht, The Netherlands
[c] Faculty of Psychology and Education Sciences, University of Coimbra, Coimbra, Portugal
[d] NeuroImaging Center, University Medical Center Groningen, University of Groningen, Groningen, The Netherlands

ARTICLE INFO

Article history:
Received 1 November 2016
Received in revised form
2 August 2017
Accepted 28 August 2017
Available online 1 September 2017

Keywords:
Resting state fMRI
Visual cortex
Phase synchronization

ABSTRACT

Resting-state fMRI is widely used to study brain function and connectivity. However, interpreting patterns of resting state (RS) fMRI activity remains challenging as they may arise from different neuronal mechanisms than those triggered by exogenous events. Currently, this limits the use of RS-fMRI for understanding cortical function in health and disease. Here, we examine the phase synchronization (PS) properties of blood-oxygen level dependent (BOLD) signals obtained during visual field mapping (VFM) and RS with 7T fMRI. This data-driven approach exploits spatiotemporal covariations in the phase of BOLD recordings to establish the presence of clusters of synchronized activity. We find that, in both VFM and RS data, selecting the most synchronized neighboring recording sites identifies spatially localized PS clusters that follow the topographic organization of the visual cortex. However, in activity obtained during VFM, PS is spatially more extensive than in RS activity, likely reflecting stimulus-driven interactions between local responses. Nevertheless, the similarity of the PS clusters obtained for RS and stimulus-driven fMRI suggest that they share a common neuroanatomical origin. Our finding justifies and facilitates direct comparison of RS and stimulus-evoked activity.

© 2017 Elsevier Inc. All rights reserved.

1. Introduction

Resting state (RS) fMRI is a popular method to examine brain function and connectivity in health and disease. Blood-oxygen level dependent (BOLD) fluctuations exhibit extensive spatial structure during RS, making RS-fMRI a valuable measure of brain function and metabolism (Raichle, 2015; Vincent et al., 2007; Yeo et al., 2011). It is also becoming an increasingly important measure in clinical diagnosis (Fox, 2010; Lee et al., 2013). However, the physiological mechanisms underlying RS fMRI activity are still poorly understood. Responses at different recording sites can be correlated as a result of neuroanatomical connections, or metabolic and hemodynamic relationships (Buzsáki et al., 2007; Matsui et al., 2016; Logothetis et al., 2009; Tong et al., 2015). Therefore, interpretation of function and connectivity patterns estimated from RS remains challenging. Furthermore, high-resolution fMRI and methods to analyze patterns of neuronal responses on the cortical surface are becoming increasingly common, particularly in vision research (Aquino et al., 2012; Dumoulin and Wandell, 2008; Schira et al., 2009; Haak et al., 2013). This creates a need for methods that can adequately describe the interactions between structural connections, neuronal metabolism and hemodynamics at the cortical surface level.

Previous studies have examined the structure of occipital BOLD fluctuations in RS and shown that they are influenced by several factors: local spatial fluctuations within visual field maps that may reflect aggregate population activity (Butt et al., 2013; Heinzle et al., 2011; Parker et al., 2016), widespread iso-eccentric fluctuations within and between visual areas (Arcaro et al., 2015; Yeo et al., 2011; Butt et al., 2015) that may partly reflect the transition between foveal and peripheral regions (Bock et al., 2015), and visuotopically organized co-fluctuations between visual areas (Raemaekers et al., 2014; Gravel et al., 2014; Bock et al., 2015; Heinzle et al., 2011), which may reflect links between neuronal populations sharing the same visual field selectivity within and across areas. However, the neuronal correlates of these components, their functional relevance, and their interactions are not yet fully understood. For this reason, demonstrating that patterns of BOLD responses derived from both stimulus-driven and spontaneous

* Corresponding author.
E-mail address: nicolas.gravel@gmail.com (N. Gravel).

https://doi.org/10.1016/j.neuroimage.2017.08.063
1053-8119/© 2017 Elsevier Inc. All rights reserved.

brain activity can be parcelled into similar, spatially specific motifs would provide valuable insights into the neuronal correlates underlying RS-fMRI activity.

Here, we take a new approach by investigating the spatial structure that arises from local covariations in the phase of low-frequency BOLD fluctuations within early visual cortex. First, we ask whether clustering based on such phase synchronization (PS) analysis establishes modular spatial structure. Next, we ask whether the synchronization clusters derived from signals recorded during RS and VFM are similar. Finally, we examine whether synchronization between clusters with similar visual field position selectivity across visual areas reflects the underlying layout of neuroanatomical connections, which may provide clues to their origin.

To establish and quantify the spatial structure of PS we take a modeling approach in which we analyze how PS and clustering change with cortical and visuotopic distance. Together, this lets us characterize the spatial extent of local synchrony and parcelate recording sites into topographically localized clusters.

To preview our main finding, we find that clustering the phase covariations in both RS and VFM results in discrete topographically organized synchronization clusters that are stable across sessions and conditions (VFM and RS). This suggests that the synchronization clusters obtained from both RS and VFM activity are subserved by common neuroanatomical underpinnings.

2. Methods

2.1. Data

The empirical data used in the main body of this paper has previously been described in Gravel et al. (2014). The main results were replicated using a second data set that has previously been described in Raemaekers et al. (2014). The methods and results for this second dataset are presented in the supplementary information.

2.1.1. Participants

Data was acquired for four participants with normal visual acuity (age: S1 = 26, S2 = 30, S3 = 31,S4 = 40). Experimental procedures were approved by the medical ethics committee of the University Medical Center Utrecht.

2.1.2. Visual field mapping stimulus

Visual stimuli were presented by back-projection onto a 15.0 × 7.9 cm gamma-corrected screen inside the MRI bore. The subject viewed the display through prisms and mirrors, and the total distance from the subjects eyes (in the scanner) to the display screen was 36 cm. Visible display resolution was 1024 × 538 pixels. The stimuli were generated in Matlab (Mathworks, Natick, MA, USA) using the PsychToolbox (Brainard, 1997; Pelli, 1997). The visual field mapping paradigm consisted of drifting bar apertures at various orientations, which exposed a 100% contrast checkerboard (switching contrast at 5 Hz) moving parallel to the bar orientation. After each horizontal or vertical bar orientation pass, 30 s of mean-luminance stimulus were displayed. Throughout the VFM, subjects fixated a dot in the center of the visual stimulus. The dot changed color between red and green at random intervals. To ensure attention was maintained, subjects pressed a button on a response box every time the color changed. Detailed procedures can be found in (Dumoulin and Wandell, 2008) and (Harvey and Dumoulin, 2011). The radius of the stimulation area covered 6.25° (eccentricity) of visual angle from the fixation point.

2.1.3. Resting state

During the resting state scans, the stimulus was replaced with a black screen and subjects closed their eyes. The lights in the scanning room were off and blackout blinds removed light from outside the room. The room was in complete darkness. Thus, visual stimulation was minimized. The subjects were instructed to think of nothing in particular and not to fall asleep.

2.1.4. MRI acquisition

Functional T2*-weighted 2D echo planar images were acquired on a 7 T scanner (Philips, Best, Netherlands) using a 32 channel head coil at a voxel resolution of 1.98 × 1.98 × 2.00 mm, with a field of view of 190 × 190 × 50 mm. TR was 1500 ms, TE was 25 ms, and flip angle was set to 80°. The volume orientation was approximately perpendicular to the calcarine sulcus. In total, eight 240-volumes functional scans were acquired, comprising 5 resting state scans (RS) interleaved with 3 VFM scans (first was an RS scan). High resolution T1-weighted structural images were acquired at a resolution of 0.49 × 0.49 × 0.80 mm, with a field of view of 252 × 252 × 190 mm. TR was 7 ms, TE was 2.84 ms, and flip angle was 8°. We compensated for intensity gradients across the image using an MP2RAGE sequence, dividing the T1 by a co-acquired proton density scan of the same resolution, with a TR of 5.8 ms, TE was 2.84 ms, and flip angle was 1°. Physiological recordings were not collected.

2.1.5. Preprocessing

First, the T1-weighted structural volumes were resampled to 1 mm isotropic voxel resolution. Gray and white matter were automatically labeled using Freesurfer and labels were manually edited in ITKGray to minimize segmentation errors (Teo et al., 1997). The cortical surface was reconstructed at the white/gray matter boundary and rendered as a smoothed 3D mesh (Wandell et al., 2000). Motion correction within and between scans was applied for the VFM and the RS scans (Nestares and Heeger, 2000). Subsequently, data were aligned to the anatomical scans and interpolated to the anatomical segmentation space (Nestares and Heeger, 2000). Instrumental drift was removed by detrending with a discrete cosine transform (DCT) filter with cutoff frequency of 0.01 Hz. In order to reduce nuisance from high frequency physiological variation, the detrended signals were filtered with a low-pass 4th order Butterworth filter with cutoff frequency of 0.1 Hz. The resulting signals were used for population receptive field (pRF) modeling (Section 2.2.1). Additionally, in order to analyze narrow band low-frequency synchronization patterns (Section 2.2.2), detrended signals were band-pass filtered using two 4th order bandpass Butterworth filter with cutoff 0.04 Hz and 0.07 Hz (Glerean et al., 2012).

2.2. Analysis

2.2.1. Visual field mapping

Visual field maps V1, V2, and V3 were mapped using the pRF method (Dumoulin and Wandell, 2008). This summarizes the visual field position to which each recording site responds as a circular Gaussian in visual space. An isotropic 2D Gaussian was chosen as pRF shape characterized by three parameters: x and y (position), and size (sigma). Here, a large set of candidate pRF models are combined with the stimulus aperture to generate predictions of the neuronal responses each candidate pRF would produce. This predicted neuronal response time course is convolved with the hemodynamic response function (HRF) to give a set of candidate predicted fMRI response time courses for each combination of pRF parameters. The best fitting predicted fMRI time course and its associated pRF parameters are then chosen to summarize the response of each recording site, together with the model variance explained to summarize the model goodness of fit (Dumoulin and Wandell, 2008). Recording sites were excluded from subsequent analyses if their best fitting pRF models explained less than 30% of response variance, or had visual field eccentricities beyond 6°.

2.2.2. Estimating phase synchronization

To establish the degree of synchronization of low-frequency

BOLD fluctuations, we estimated the phase locking values (PLV) of the BOLD signals of all pairs of recording sites within a visual field map. The PLV is a measure of phase synchronization widely described in the literature (Tass et al., 1998; Lachaux et al., 1999) and it has been used in fMRI (Glerean et al., 2012; Laird et al., 2002; Ponce-Alvarez et al., 2015). We first obtained estimates of the instantaneous phase of the band-pass filtered BOLD signal by computing the Hilbert transform and then taking the angle of the resulting analytical signal (Laird et al., 2001). Data were bandpass filtered because instantaneous phase estimates thus obtained only admit clear physical interpretation for a narrow frequency band. After obtaining instantaneous phase estimates for each recording site at each time point, we discarded the 5 first and 5 last time points (the first and last 7.5 s of recording) to avoid edge effects inherent to the Hilbert transform. Afterwards, we computed the PLV matrix by using the following equation:

$$PLV_{i,j} = \frac{1}{T}\left|\sum_{t=1}^{T} e^{i\Delta\varphi_{i,j}(t)}\right| \quad (1)$$

where $PLV_{i,j}$ represents the time averaged symmetric phase locking values matrix between the recording sites i,j; $\Delta\phi_{i,j}(t)$ is the instantaneous phase difference between any two recording sites at time t and T is the total duration of the recording. This matrix summarizes the average synchronization tendency of low-frequency BOLD fluctuations over the scanning session.

2.2.3. Parcellation into synchronization clusters

To identify the spatial structure that arises from local covariations in the phase of low-frequency BOLD fluctuations, we searched for groups of neighboring recording sites (contiguous along the grid defined by the cortical surface reconstruction) that were, on average, highly synchronous during the entire duration of a scan. This was achieved by selecting the 5% strongest entries in the PLV matrix. Afterwards, we pruned the 5% strongest entries in the PLV matrix by setting the synchronization values of recording sites beyond 3 mm distance to zero. The cortical distances between recording sites were estimated as the shortest distance along the cortical surface manifold using Dijkstras algorithm (Dijkstra, 1959) (Dijkstra, 1959). We choose a 3 mm distance threshold to emphasize short range (local, contiguous along the cortical surface) over long range (large-scale, between distant cortical folds) interactions. Pruning the PLV matrix before clustering helped minimize the contribution of long-range interactions while emphasizing local interaction structure. This implies that two distant voxels could be assigned to the same cluster only if they were chained together through synchronized neighbors.

Next, we clustered the pruned PLV matrix using the Louvain clustering algorithm (Blondel et al., 2008). The Louvain algorithm finds the optimal modular partition of non-overlapping clusters by maximizing the number of within-cluster connections while minimizing the number of between-cluster connections. The algorithm depends on a scaling parameter that determines the scale of the modular partition, which we set to 1, the default value defined for classic modularity (Rubinov and Sporns, 2010). Due to the non-deterministic nature of the clustering algorithm, slightly different solutions are obtained each time the algorithm is run. Therefore we applied an iterative approach. First, we run the Louvain clustering algorithm 10 times and then calculated an agreement matrix for all iterations. The entries in this matrix indicate the probability that a link was assigned to the same partition across all iterations. Next, we run the clustering algorithm another 10 times on the most probable entries of the agreement matrix (agreement >0.9). This approach converges to the most probable modular partition (Betzel et al., 2013) for each VFM and RS scan. Lastly, we computed a consensus partition from the resulting modular partitions of the individual VFM and RS scans. For illustrative purposes, we render the consensus partitions obtained from all VFM and RS scans on inflated reconstructions of the cortical surface and in visual space (using the pRF positions of the recording sites in each cluster).

2.2.4. Reproducibility of synchronization clusters

To determine whether identified PS clusters were similar across scanning sessions, we computed the normalized mutual information (NMI) between modular partitions derived from different scans. First, we computed NMI values between all scan pairs of the same category (3 VFM and 5 RS). Second, we computed the NMI between the consensus RS and VFM partitions. To demonstrate that NMI values reflected genuine features of the data (similar spatial covariations) rather than methodological artifacts, we constructed a surrogate NMI distribution under the null hypothesis that high NMI values could be obtained from data in which there are no meaningful spatial correlations (i.e. spatially randomized data). This allowed us to compare empirical NMI estimates to a baseline.

To construct the surrogate NMI distribution, we first generated 30 surrogate data sets for each visual area by permuting the indices of the grid defined by the cortical surface reconstruction. This removed the spatial structure of the data while keeping the autocovariance and temporal covariations intact. We choose to shuffle grid and not voxel space because shuffling before interpolating to gridspace can remove some extremes in the data, smoothing it out while bringing everything towards the mean (Hagler et al., 2006). Second, we computed modular partitions for each surrogate data set as we did with the empirical data. Third, we computed the NMI between these surrogate partitions and the empirical partitions, obtaining a surrogate distribution of NMI values. Finally, we compared this distribution to the empirical NMI distributions using a Mann-Whitney test. This gave the probability of observing each empirical NMI distribution by chance.

Additionally, we examined whether the size of the clusters derived from RS and VFM were similar by computing the cortical surface area of each cluster. Only recording sites directly on the white-gray matter boundary were considered for area computation. Cluster areas were then averaged for each visual field map and hemisphere, giving a total of 24 averages for VFM and RS. We used the Pearson correlation coefficient between average cluster areas derived from RS and VFM data to compare their similarity.

2.2.5. Visuotopic organization of phase synchronization clusters

To examine the visuotopic organization of clusters, we investigated how the probability of any two recording sites sharing a cluster changed as a function of the visual field distance between their population receptive fields (pRF). For all visual field maps, hemispheres and subjects, we computed the binomial probability of sharing a cluster for the RS-derived consensus partition for bins of 0.25° of visual field distance. The visual field distances between all recording pairs were estimated in the radial and angular directions as the difference in their corresponding pRF eccentricities and arc distance, respectively. The arc distance was computed by multiplying the pRF polar angle difference with the average pRF eccentricity of any two recording sites. To estimate how the range of cluster membership probability changes with radial and arc distance we fitted binomial distributions with the radial and arc distances as independent variables, and computed the decay factor of these probabilities. To ensure probabilities were computed between truly adjacent locations, only arc distances between iso-eccentric and radial distances between iso-angular locations were considered (a tolerance of 2° was used).

2.2.6. Spatial extent of phase synchronization

We also determined the spatial extent of phase synchronization (PS) by estimating how it decreases with cortical and visuotopic distance. First, for each visual field map, subject and scan, we

computed the average PLV for every 1 mm increase in cortical distance. We then quantified the spatial extent of PS by drawing on a framework developed in geophysics for the empirical evaluation of spatial dependencies: the variogram (Ye et al., 2015; Parker et al., 2016). The variogram provides a measure of how much two samples vary depending on their distance. In order to adapt the method to describe the dependency of the PLV with cortical distance, we proceeded as follows. First, we defined an exponential model by centering an exponential function at zero distance and keeping its maximum amplitude at 1, the maximum possible value for the PLV. We then varied the decay factor (in mm of cortical distance), and the baseline PLV of this exponential model to fit the distance-binned PLV data. We choose the exponential model because the relation between functional connectivity and cortical distance is well described by an exponential decay (Butt et al., 2013) and because the models parameters have a direct physical interpretation, in millimeters of cortical distance and PS magnitude (PLV). This allowed us to summarize the spatial extent of the aggregate synchronous activity contributed by a set of neighboring recording sites (synchronization range) and their long range baseline interactions (baseline). One important difference between our approach and variogram analysis as applied in geophysics is that here we use the decay factor as a measure of the synchronization range. In a standard variogram analysis, the range corresponds to 3 times the decay factor and roughly describes the region in which spatial correlations dissipate into randomness (here baseline). Synchronization range (the decay factor) and baseline were estimated for each subject, scan and visual area separately.

Additionally, we examined how PS decreases with visuotopic distance. Similarly as previously described, for each visual field map combination (V1-V1, V2-V2, V3-V3, V1-V2, V1-V3 and V2-V3), subject and scan, we computed the average PLV for every 1° increase in visuotopic distance. Visuotopic distances were computed using the following equation:

$$D_{i,j} = \sqrt{r_i^2 + r_j^2 - 2r_i^2 r_j^2 cos(\theta_i - \theta_j)} \quad (2)$$

where *D(i,j)* represents the visuotopic distance between the recording sites *i,j*. As explained previously, we modeled the range and baseline of PS in visual space by using an exponential decay function. To test for differences in range and baseline between VFM and RS derived estimates, we computed two sample t-tests. To test whether there was a correlation between synchronization range and the cortical areas (in mm) of the synchronization clusters in different scans, we computed the Pearson correlation between the synchronization range and cluster cortical areas for data grouped across subjects, visual areas and scans (5 for RS and 3 for VFM).

2.2.7. Intra and inter-hemispheric cluster connectivity

We examined whether clusters sharing similar visual field selectivity have higher PLV across areas and hemispheres. To answer this, we proceeded as follows. Clusters were first grouped over foveal and peripheral quarter-fields using the averaged eccentricity and polar angle pRF preferences of their cortical grid points. The transition between fovea and periphery was set to 2.2°. The grouping process resulted in a matrix of 24 ROIs, 4 for each area (V1, V2 and V3) in each hemisphere. Signals for each ROI were obtained by averaging the minimally preprocessed signals (after detrending) and filtering in the in the 0.04–0.07 Hz. From these signals, the PLV was computed resulting in 24 × 24 PLV matrices for each subject, scan and condition (12 × hemisphere). These matrices were then averaged over scans and the resulting grand averages classified as intra- or inter-hemispheric functional connections. Subsequently, these connections were z-scored (separately) and evaluated for significance across subjects using permutations corrected for multiple comparisons. We then asked if the resulting PLV-based functional connectivity matrices matched the underlying homotopic anatomical connections. For this purpose, we created a binary matrix with ones indicating homotopic connections between foveal and peripheral quarter-fields in different areas and hemispheres and used the Spearman correlation between the PLV-based connectivity matrices and the matrix representing homotopic anatomical connections.

3. Results

3.1. Synchronization clusters derived from resting state and visual field mapping

We first asked two questions: 1) whether spatially localized patterns of functional connectivity within visual areas could be derived from resting state (RS) data; and 2) whether these patterns were similar to those evoked by visual field mapping (VFM) stimuli. Both in RS and VFM, clustering the 5% most synchronized neighbours revealed a modular network structure that maps to discrete cortical regions that group recording sites with similar eccentricity and polar angle preference. Fig. 1 shows the parcellation based on the consensus clustering across individual scans in both RS and VFM for one participant. PS clusters obtained from one RS scan were significantly more similar to those from another RS scan than they were to clusters from surrogate RS data with recording sites randomly permuted (average V1 normalized mutual information ($<$NNMI$>$ to empirical RS data was 0.744, while ⟨NMI⟩to surrogate RS data was 0.635. $p < 0.0001$. All subjects show this result in V1, V2 and V3, as shown in Supplementary Table 1). Importantly, consensus cluster partitions obtained from VFM data were significantly more similar to clusters from RS data ($<$MNI$>$ = 0.745) than they were to clusters from surrogate RS data with recording site locations randomly permuted ($<$NMI$>$ = 0.623) ($p < 0.001$) (Supplementary Table 2). These results indicate that PS clusters were stable in space both across scanning runs and different conditions. The average cortical surface area of clusters derived from VFM and RS was strongly correlated (Pearson correlation coefficient $r = 0.94$, $p < 10^{-11}$) but clusters were significantly larger in VFM than in RS ($p = 0.0045$) (Fig. 2A).

3.2. Visuotopic organization of synchronization clusters

Next, we examined the visuotopic organization of synchronization clusters to test whether the clustering reflects neuronal response preferences of the recording sites. We quantified how the probability of any two recording sites sharing a cluster changed as a function of the radial and arc distances between recording sites. In both radial and angular directions, recording sites are more likely to share a cluster if their pRFs are close in visual space (Fig. 2B and C). However, the probability of sharing a cluster declines faster with visual field distance in the angular than the radial direction. Therefore, the visual field extent of clusters is elongated along the radial direction both in RS (decay factor: 1.93° for the radial direction and 0.3° for the angular direction) and in VFM (decay factor: 1.65° for the radial direction and 0.25° for the angular direction). This systematic asymmetry in the relationship between visual position preferences and clustering cannot be straightforwardly explained by relationships to cortical location.

3.3. Comparison of the spatial extent of phase synchronization between RS and VFM

We next asked whether the spatial extent of phase synchronization differed between VFM and RS scans. To test this, we fit the relationship between the PLV and cortical distance as an exponential function. This help us quantifies the synchronization range and baseline (long-range) magnitude of the PLV as the decay factor and offset, respectively (Fig. 3). Across subjects and scans, in V1, V2 and V3, the

synchronization range spread over a larger cortical distance in VFM (mean (SD): V1 = 7.72 mm (0.75); V2 = 7.81 mm (1.13) and V3 = 7.92 mm (1.79)) than in RS (mean (SD): V1 = 3.19 mm (1.17); V2 = 2.97 mm (1.41) and V3 = 3.11 mm (0.86)). In VFM, baseline synchronization estimates were smaller (mean (SD): V1 = 0.24 (0.022); V2 = 0.37 (0.07) and V3 = 0.36 (0.09)) than those for RS (mean (SD): V1 = 0.46 (0.069); V2 = 0.45 (0.068) and V3 = 0.45 (0.11)). Differences between VFM and RS derived synchronization range and baseline were significant in all cases (two sample *t*-test: $p < 10\text{-}5$ for V1; $p = 0.0252$ for V2; $p = 0.0307$ for V3). Next, we asked how phase synchronization changed between voxels, within and between areas, with close visuotopic selectivity in VFM and RS.Similarly to what we previously described, we fit an exponential function to the relationship between the PLV and visuotopic distance instead (Fig. 4). Across subjects and scans, within V1, V2, V3 and between V1-V2, V1-V3 and V2-V3, the synchronization range spread over a larger visuotopic distance (in degrees of visual angle) in VFM (mean (SD): V1 = 0.99° (0.14); V2 = 1° (0.13); V3 = 0.95° (0.19); V1-V2 = 0.97° (0.14); V1-V3 = 0.89° (0.15) and V2-V3 = 0.94° (0.14)) than in RS (mean (SD): V1 = 0.45° (0.17); V2 = 0.51° (0.16); V3 = 0.44° (0.22); V1-V2 = 0.42° (0.18); V1-V3 = 0.32° (0.18) and V2-V3 = 0.41° (0.21)). In VFM, baseline synchronization estimates were smaller (mean (SD): V1 = 0.21 (0.013); V2 = 0.22 (0.017); V3 = 0.24 (0.024); V1-V2 = 0.22 (0.013); V1-V3 = 0.23 (0.015) and V2-V3 = 0.23 (0.011)) than those for RS (mean (SD): V1 = 0.45 (0.08); V2 = 0.39 (0.08); V3 = 0.43 (0.11); V1-V2 = 0.39 (0.073); V1-V3 = 0.38 (0.074) and V2-V3 = 0.4 (0.095))). Differences between VFM and RS derived synchronization range and baseline were significant in all cases (two sample *t*-test: $p < 10\text{-}5$ for all cases). Finally, we asked whether there was a correlation between synchronization range and the areas of the synchronization clusters in different RS scans. To this end, we computed the Pearson correlation between the synchronization range and the mean cluster areas for data grouped across subject, resting state scans and visual areas. For cortical distances, we found no significant correlation between synchronization range and mean cluster areas ($r = -0.044$, $p = 0.737$, $n = 60$). For visuotopic distances, we found a weak correlation ($r = 0.31$, $p = 0.0128$, $n = 60$).

3.4. Homotopic anatomical connectivity of cluster synchronization

We also asked whether clusters sharing similar visual field selectivity had higher PLV across visual areas and hemispheres. To answer this, we grouped the data in each hemisphere across upper/lower foveal and peripheral quadrants and computed significant PLV-based functional (intra- and inter-hemispheric)connections for RS and VFM data ($p < 0.001$, permutations corrected for multiple comparisons. See Fig. 5). The resulting binary matrices were compared to a binary matrix consisting of connections between ROIs with similar visuotopic selectivity using Spearman correlation (intra-hemispheric: 0.45 for RS and 0.56 for VFM. Inter-hemispheric: 0.46 for RS and 0.57 for VFM. $p < 0.0001$ for all cases). The match between PLV-based functional connections and anatomical connections increased in VFM.

4. Discussion

Using covariations in local phase synchrony to parcelate the fMRI signal, we revealed a stable spatial structure in BOLD fluctuations recorded during resting state (RS). This spatial structure, which we identified as phase synchronization (PS) clusters, was also observed in response to visual field mapping (VFM) stimuli. Interestingly, the magnitude and spatial extent of PS varied in different RS scans yet the shape, elongated along eccentricity, and location of the PS clusters remained stable. Importantly, the topographical organization of synchronized hemodynamic activity across areas strongly reflected the layout of homotopic anatomical connections. The similar shape and location of the PS clusters obtained for RS and stimulus-driven fMRI, together with the high synchrony between clusters sharing similar visual field position selectivity across visual cortical areas and hemispheres, suggest that they share a common neuroanatomical origin. Therefore, our findings justify and facilitate direct comparison of RS and stimulus-evoked activity.

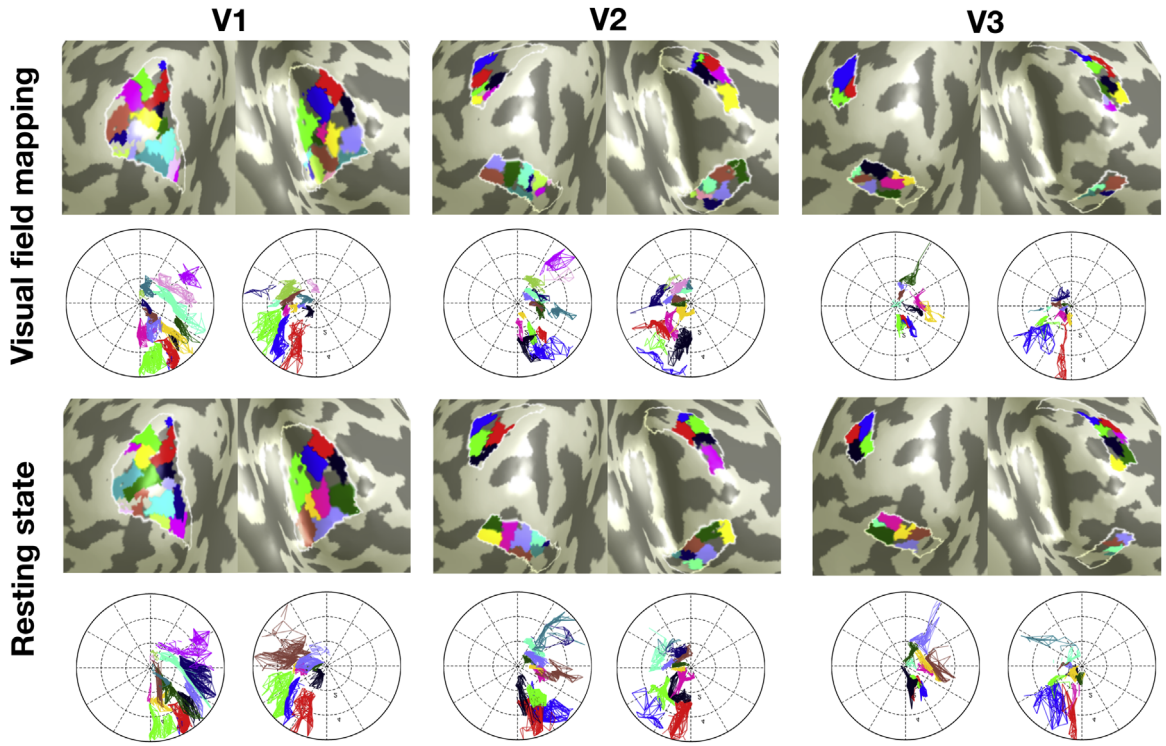

Fig. 1. Consensus synchronization clusters obtained for all VFM and RS scans of a single subject (results for other subjects are included in supplementary materials Figs. 1S and 5S). Modules depicted in the cortical surface reconstruction and in visual space (their perimeter) using each recording sites pRF position. Different clusters are shown in different colors, which correspond between cortical surface and visual field representations (recording sites within 0–6° of eccentricity). The number of clusters and colors may not match between RS and VFM.

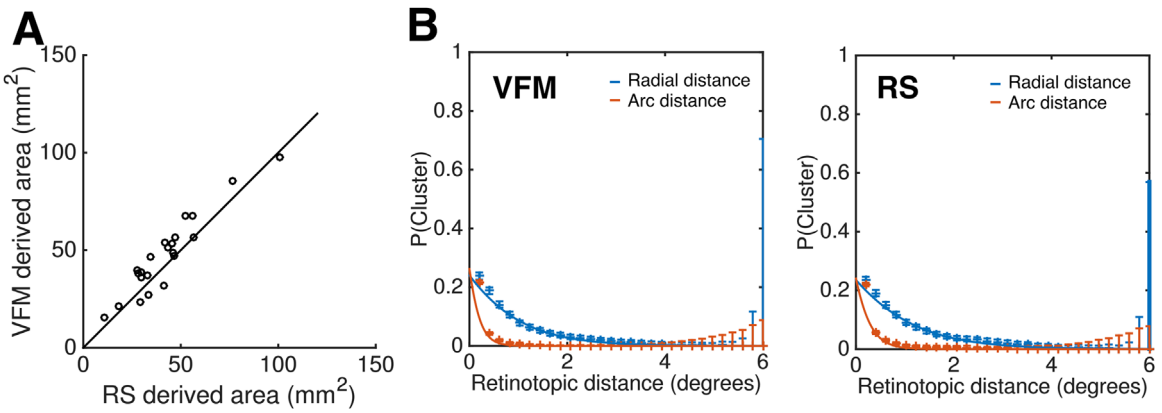

Fig. 2. Spatial aspects of the synchronization clusters. (A) Correlation between cortical surface areas of VFM and RS derived clusters. Average areas of cluster were obtained for each visual field map in each subject hemispheres. The average cortical surface area of clusters was significantly correlated ($r = 0.94$, $p < 10^{-11}$) but nevertheless were significantly larger for estimates based on VFM or RS data ($p = 0.0045$, Wilcoxon signed rank test). As most data points are distributed above the unity line, this indicates that the synchronization cluster were slightly larger when derived from the VFM data. (B) In RS, shared cluster membership probability decreases with visual field distance. The probability of two recording sites sharing a synchronization cluster decreases with the visuotopic distance between the recording sites pRFs for both the radial (blue) and the angular direction (red). The spread of shared cluster membership was greater along the radial direction (decay factor = 1.93° for RS and 1.65° for VFM) compared to the angular direction (decay factor = 0.3° for RS and 0.25° for VFM). Error bars correspond to the binomial probability and its confidence interval for bins of 0.25° of visuotopic distance. The continuous trace corresponds to the binomial probability fit of all data within 0–6° of visuotopic distance. The binomial fits were obtained after grouping the data over areas, scans, subjects and conditions. (C) Same as in (B) but for the VFM data.

4.1. Phase-synchronization-based parcellation of RS fMRI signals reveals topographically organized clusters in early visual cortex

Analyzing the phase synchronization (PS) of low-frequency BOLD fluctuations within early visual cortex, we revealed synchronization clusters during resting state (RS). The spatial structure was consistent among different RS scans, indicating that within-area local interactions are preserved during RS. This within-area stability is in contrast to the variability in between-area interactions observed in previous studies (Heinzle et al., 2011; Raemaekers et al., 2014; Butt et al., 2013; Gravel et al., 2014). Whereas between-area interactions are less stable during RS, during VFM they become more stable (Gravel et al., 2014; Arcaro et al., 2015; Heinzle et al., 2011; Roseman et al., 2016), giving rise to a synchronization-based structure that is consistently found across subjects (as shown by Fig. 5). Both in RS and VFM, the PLV structure resembled the layout of homotopic anatomical connections (cortical connections between visual areas sharing similar visual field position selectivity) within and between hemispheres (Fig. 5). The finding that across-area cluster synchronization follows the underlying layout of homotopic anatomical connections points to a structural anchoring in spontaneous fMRI activity.

4.2. Similar location and shape, but different spatial extent of phase synchronization clusters for resting state and visual field mapping

Similar cluster structure was observed in BOLD activity during RS and in response to visual field mapping (VFM) stimuli. However, the PS clusters found in VFM were slightly larger than those found in RS (Fig. 2A). This mirrors our result that synchronization range spreads over a larger cortical extent in VFM, but local variations in the magnitude and spatial extent of PS do not affect the overall location and shape of the PS clusters. The fact that PS between neighboring recording sites (i.e. synchronization range) decreases more gradually with cortical and visual distance in VFM than in RS likely reflects a stimulus-evoked increase in spatial interactions (Lacy et al., 2016; Schellekens et al., 2013). The narrower synchronization range in RS data is consistent with recent findings demonstrating that within- and between-area interactions in primary and extrastriate visual areas have a narrower spatial footprint during RS than during VFM (Heinzle et al.,

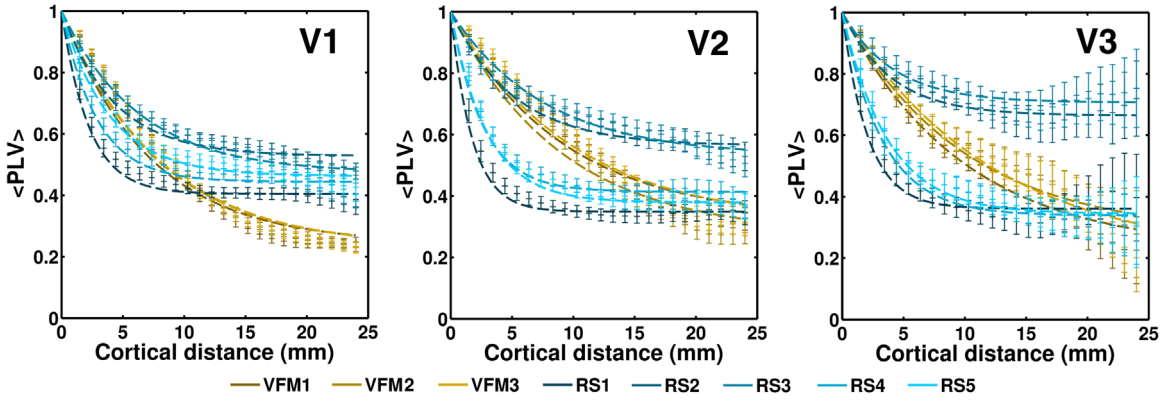

Fig. 3. Phase synchronization as a function of cortical distance in areas V1, V2 and V3. In VFM, phase synchronization range spread over a larger cortical distance than in RS scans, likely reflecting stimulus induced interactions. In contrast, in RS, baseline synchronization is higher, possibly indicating increased long range interactions or the effect of global signals. To quantify range and baseline, we fit an exponential function (dotted lines) to the average PLV binned by cortical distance (colored points). Error bars show the standard error of the mean corrected for upsampling the functional data to the reconstructed cortical surface grid (upsampling factor = 8). Across scans, in V1, V2 and V3, the synchronization range spread over a larger cortical distance in VFM (mean (SD): V1 = 7.66 mm (0.40); V2 = 9.31 mm (0.49) and V3 = 10.66 mm (1.34)) than in RS (mean (SD): V1 = 3.91 mm (1.55); V2 = 4.00 mm (2.35) and V3 = 3.45 mm (0.83)). In VFM, baseline synchronization estimates were smaller (mean (SD): V1 = 0.23 (0.007); V2 = 0.30 (0.026) and V3 = 0.23 (0.039)) than those for RS (mean (SD): V1 = 0.46 (0.045); V2 = 0.44 (0.095) and V3 = 0.48 (0.18)). Differences between VFM and RS derived synchronization range and baseline estimates were significant in all cases ($p < 0.05$, two sample *t*-test). Global average PLV floor, computed by permuting voxel indexes across subjects and scans, was: 0.33 for VFM scans and 0.42 for RS scans. Data for a single subject. Data for other subjects are included in the supplementary material (Fig. 3S).

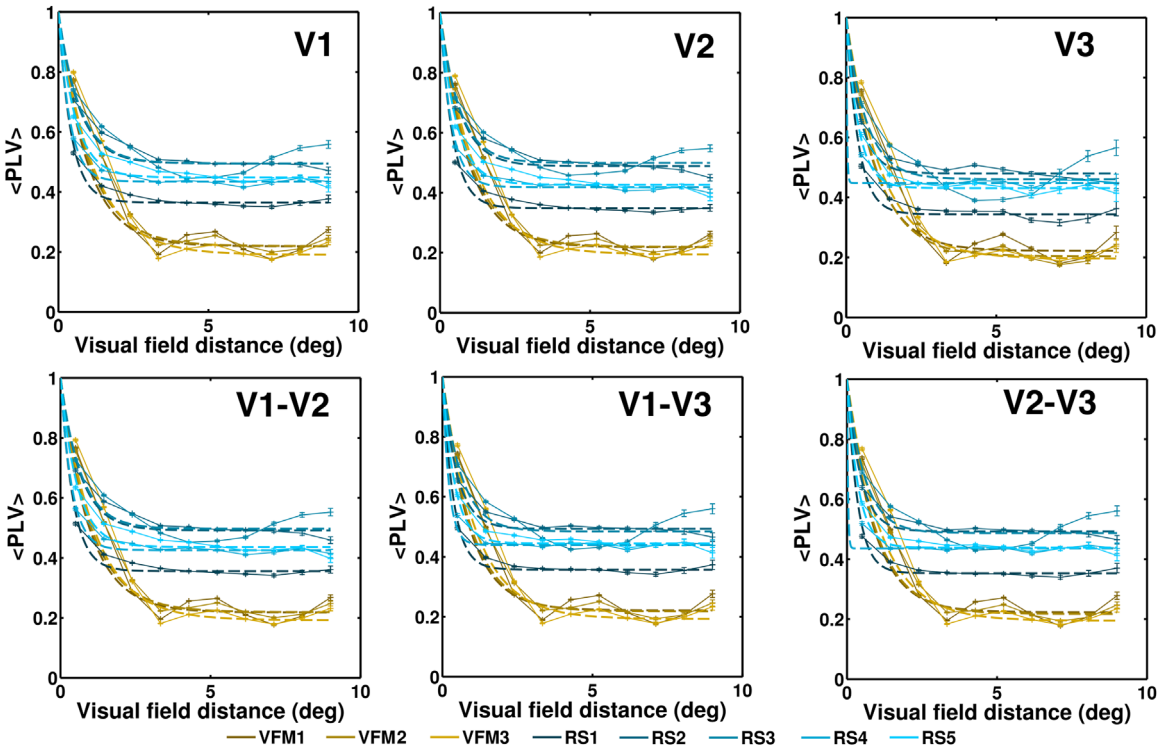

Fig. 4. Phase synchronization as a function of visuotopic distance for areas V1, V2 and V3. Phase synchronization, expressed as PLV, was grouped from 0 to 10° in bins of 1°. Points represents the voxel averages across bins for each scan. To quantify differences between VFM and RS we fit an exponential function to the average PLV binned by visuotopic distance and compute the range and baseline. Across scans, within V1, V2, V3 and between V1-V2, V1-V3 and V2-V3, the synchronization range spread over a larger visuotopic distance (in degrees of visual angle) in VFM (mean (SD): V1 = 1.02° (0.1); V2 = 0.98° (0.05); V3 = 1.04° (0.2); V1-V2 = 0.97° (0.09); V1-V3 = 0.94° (0.12) and V2-V3 = 0.98° (0.07)) than in RS (mean (SD): V1 = 0.55° (0.15); V2 = 0.47° (0.088); V3 = 0.38° (0.099); V1-V2 = 0.43° (0.22); V1-V3 = 0.36° (0.13) and V2-V3 = 0.38° (0.075)). In VFM, baseline synchronization estimates were smaller (mean (SD): V1 = 0.21 (0.016); V2 = 0.21 (0.016); V3 = 0.22 (0.04); V1-V2 = 0.20 (0.012); V1-V3 = 0.21 (0.014) and V2-V3 = 0.22 (0.089)) than those for RS (mean (SD): V1 = 0.44 (0.053); V2 = 0.43 (0.13); V3 = 0.48 (0.16); V1-V2 = 0.37 (0.088); V1-V3 = 0.36 (0.1) and V2-V3 = 0.44 (0.14))). Differences between VFM and RS derived synchronization range and baseline were significant in all cases (two sample *t*-test: $p < 10\text{-}5$ for all cases). Data for a single subject. Data for other subjects are included in the supplementary material (Fig. 4S).

2011; Raemaekers et al., 2014; Butt et al., 2013; Gravel et al., 2014). However, long range (baseline) PLV interactions were higher during RS, possibly indicating increased long-range interactions or global activity. In some RS scans, between ROI interactions in PS resembled those seen in visual field mapping. Interestingly, in a previous study of the first dataset, connective field models computed from those scans revealed well-ordered topographic maps (Gravel et al., 2014).

An interesting feature of the cluster shape is its radial-tangential anisotropy. PS clusters derived from both RS and VFM are radially elongated in the visual field maps (Fig. 2B and C). One possible factor for this elongation is a certain non-uniformity introduced by the shape of the ROIs. However, the ROIs are not always elongated (while V2 and V3 quarter fields sometimes are, V1 quarter fields generally not). Moreover, clusters are too small to be affected by ROI shape. Another possibility is that, due to the log-scaling between visual field and cortical coordinates (Schira et al., 2010), circular connectivity on the cortical surface may look radially elongated when depicted in visual space (Nandy and Tjan, 2012; Toet and Levi, 1992). To explore these possibilities, we smoothed the time series using a 2D Gaussian kernel (2 and 15 mm FWHM, Fig. 2S in supplementary material) defined onto the reconstructed cortical surface (grid). Anisotropy was preserved but its range widened with smoothing. We also modeled the effect of circular connectivity (without using the time series) on anisotropy by clustering toy models of circular connectivity on the cortical surface. Two toy cases were considered: 1) a matrix of weights constructed by assigning a 2 mm FWHM Gaussian connectivity profile to each location; and, 2) a binary network of nearest neighbors chains (3 mm and 6 mm threshold). Anisotropic clusters with similar spatial ranges were recovered in both cases. Clusters obtained from a shuffled grid (were 2D spatial relations are destroyed) did not show anisotropy (Fig. 2S in supplementary materials). In sum, all lines of evidence seem to support the second option: circular connectivity on the cortical surface looks elongated in visual space. This cluster elongation in the eccentricity direction may have functional consequences. One hypothetical functional structure that has a similar radially elongated shape is the so-called integration field identified by crowding research (Kooi et al., 1994; Toet and Levi, 1992; Bouma, 1970; Pelli, 2008; Nandy and Tjan, 2012). Crowding is the breakdown of object recognition in peripheral vision when similar objects are too closely spaced, which increases perceptual uncertainty. It has been speculated that spacing effects on perceptual uncertainty at the behavioral level are a result of signal correlations in neuronal populations (van den Berg et al., 2012).

Besides differences in cluster size and synchronization range, RS and VFM data also differ in the decay factor of the phase locking values (PLV) with cortical distance (Fig. 3). For VFM, the PLV was very stable over scans whereas in RS it was rather variable. Searching for the origin of this variability, we re-analyzed the data after having applied global signal regression. This suppressed the long-range variability in particular in the RS data, suggesting that large-scale interactions across areas and global systemic variations affect the baseline synchronization level in each scan. We conclude that these are an important component of the observed variability in occipital RS recordings. Another cause of variability, at the behavioral level, could be the relationship between resting state BOLD fluctuations and oculo-motor behaviour that occurs subliminally and spontaneously during the scanning sessions (Ramot et al., 2011).

Hence, while we derive similar synchronization clusters from RS and VFM in terms of their location and shape, the magnitude and spatial extent of PS differs between RS and VFM data. Despite local variations in the magnitude and spatial extent of PS during

different scans and conditions, the location and shape of PS clusters is stable, demonstrating that PS clusters reflect a stable architectural property. In addition, we show that the topographical organization of synchronized hemodynamic activity across areas strongly reflects the layout of homotopic anatomical connections. Taken together, these findings support the hypothesis that spontaneous fMRI activity reflects the organization of the underlying anatomical connections (Vincent et al., 2007; Kenet et al., 2003; Tsodyks et al., 1999; Honey et al., 2009).

4.3. Spatial extent of phase synchrony during resting state: possible mechanisms

But which mechanisms could underlie the stability and spatial organization of PS? The observed spatial specificity of the spontaneous BOLD fluctuations can only emerge if the intrinsic neuronal activity within and across visual cortical areas is topographically organized. However, the neuronal basis of these BOLD patterns is not yet fully understood. It is debated on whether spontaneous fMRI activity reflects the consequences of population spiking activity, sub-threshold neuronal activity (Logothetis et al., 2001), or metabolic relationships between neurons and astrocytes (i.e. neuro-vascular coupling) (OHerron et al., 2016; Pang et al., 2017). On the one hand, BOLD phase synchronization patterns may reflect the consequences of intrinsic switching of spiking input activity to aggregate neuronal assemblies sharing similar visual field position selectivity and tuning characteristics (Kenet et al., 2003; Blumenfeld et al., 2006; Lewis et al., 2016; Vinck and Bosman, 2016). Alternatively, those patterns may be the footprint of slow subthreshold fluctuations in local field potentials, which can be visuotopically organized and good predictors of the BOLD signal (Logothetis and Wandell, 2004; Carandini et al., 2015). A recent study by Matsui and colleagues (Matsui et al., 2016) using neuronal calcium signals and simultaneous hemodynamic recordings unifies these contrasting findings by showing that both global fluctuations, in the form of propagating waves, and transient local coactivations are necessary for setting the spatial structure of hemodynamic functional connectivity (Matsui et al., 2016; Pisauro et al., 2013). Also important is the role of astrocytes, the main link between neuronal metabolism and blood flow. They certainly play a role setting the pace of visuotopically organized hemodynamic fluctuations, as it is has been shown they modulate the delay between neuronal activity and its hemodynamic response (Pang et al., 2017). Together, these findings suggest that multiple physiological factors may influence spontaneous hemodynamic activity in a way that gives rise to visuotopically organized fluctuations.

An anatomical factor that may influence the spatial extent of phase synchrony, and therefore the size and location of the clusters, is the density and distribution of capillary beds. Shaped by the intricate branching patterns of the supporting vascular network, inhomogeneity in the density and distribution of capillary beds may lead to varying blood perfusion and deoxyhemoglobin washout rates (Postnov et al., 2005; Aquino et al., 2012; OHerron et al., 2016). In addition to the effects exerted by the supporting vascular network, the energy expense of different populations of neurons and glial cells may covary with vessel density, structuring hemodynamic fluctuations in locally and functionally segregated neighborhoods (Tong et al., 2016; Buzsáki et al., 2007) whose responses are -on average-biased together (Kastner et al., 1999). This structured hemodynamic variability may lead to inhomogeneity in the coupling between the hemodynamic response of a recording site and the neuronal activity in the neighborhood of the site, and a concomitant bias among neighboring sites (Kamitani and Tong, 2005).

This inhomogeneity hypothesis is consistent with evidence from animal models pointing to the limits of hemodynamic measurements in neuroimaging studies. Harrison et al. (2002) demonstrated that the distribution of blood capillaries correlates with hemodynamic functional connectivity at the millimeter scale, suggesting a direct relationship between a neuronal populations metabolic demand and the density of its supporting capillary networks. In another study, Vazquez et al. (2014) delineated functional clusters of slow metabolic fluctuations across the mouse cortex, confirming a relationship between metabolic demand and capillary network density. Furthermore, simultaneous measurements of neuronal spiking, metabolic demand and vessel responses demonstrate that vessel dilatory responses are effectively coupled to spiking and metabolic activity (OHerron et al., 2016). However, they also show vascular responses to stimuli that elicit little to no neuronal activity in the surrounding tissue, revealing limitations of the link between hemodynamic and neuronal responses.

Large draining veins also affect the spatial structure of the BOLD signal. They are known to modulate the phase of nearby metabolic fluctuations (Winawer et al., 2010) with little effect on signal amplitude and reliability. On the other hand, parenchymal draining veins inside recording sites have a large modulatory effect on the amplitude of local BOLD signals, and are sometimes an order of magnitude larger

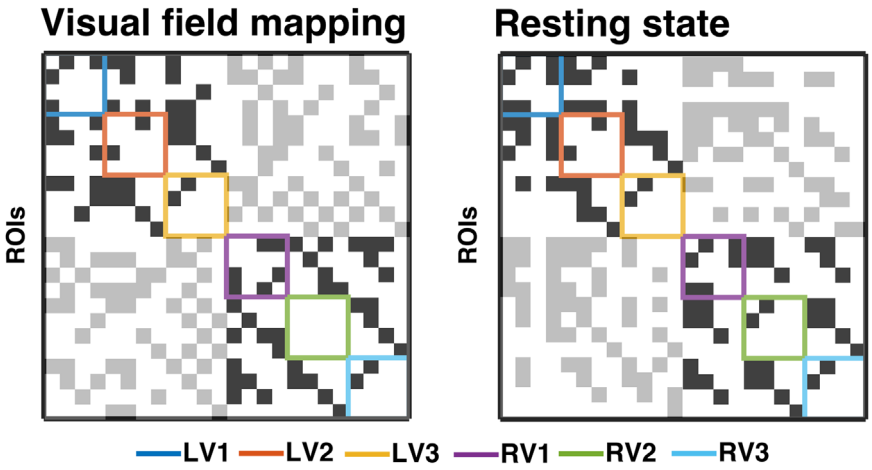

Fig. 5. Voxels in clusters with similar visual field position selectivity have higher PLV across visual field maps and hemispheres. For each subject, clusters were grouped over upper/lower foveal (below 2.2° eccentricity) and peripheral (above 2.2° eccentricity) quarter-fields and PLV matrices for intra and inter -hemispheric PLV-based functional connections were computed. Diagonal and off-diagonal quarter-fields in each matrix represent within- and between-hemisphere PLV across visual cortical areas (grouped by the colors), respectively. Inside each colored box, quarter-fields are grouped in the following order (from left to right): upper fovea, upper periphery, lower fovea and lower periphery. The resulting PLV matrices were averaged across scans and z-scored. Subsequently, a significant PLV structure across subjects (black squares for intra-hemispheric and gray squares for inter-hemispheric connections) was established using permutations ($p < 0.001$. Corrected for multiple comparisons). Furthermore, we estimated the degree of homotopy in the resulting PLV-structures by using the Spearman correlation between these and binary matrices (for within-hemisphere and between-hemisphere connections) with ones indicating homotopy (see methods section 2.2.7.). Correlations increase during VFM (intra-hemispheric: 0.45 for RS and 0.56 for VFM. Inter-hemispheric: 0.46 for RS and 0.57 for VFM. $p < 0.0001$ for all cases).

than those induced by neuronal metabolism. Pial veins, which are adjacent to the cortical surface and predominantly parallel to the sulci, similarly reduce spatial specificity and introduce noise (Winawer et al., 2010). As pial branches drain oxygen from large patches of cortex, they may play a substantial role in determining the location and shape of the synchronization clusters.

Together, these findings suggest that links between the neuronal metabolism and the hemodynamic signals have limited spatial resolution (Formisano et al., 2012; Lee et al., 1995; Menon and Kim, 1999; OHerron et al., 2016). At finer scales, vascular network structures play an important role in shaping the spatial structure of the BOLD signal. We conclude that synchronization clusters most likely reflect a combination of 1) shared metabolic demands of local neuronal populations with similar visuotopic selectivity, 2) linked neuronal activity of neuronal populations with similar visuotopic selectivity across areas, and 3) the density of supporting capillary networks, regardless of whether responses are stimulus driven or endogenous. Our findings indicate that, despite limitations in the resolution of metabolism-sensitive measurements such as fMRI to determine the contribution of neuronal activity to hemodynamic signals, it is still possible to study the neuronal properties of aggregate neuronal populations.

4.4. Limitations and future directions

We computed phase locking values (PLV) to quantify the degree of synchronization of low-frequency BOLD fluctuations despite the Pearson correlation being the most used functional connectivity measure in RS BOLD analysis. However, this is justified by two facts. Correlation values come with 2 drawbacks: First, there is an ongoing debate on how to deal with negative correlations. Second, if two signals are 90° out of phase, they will result in a Pearson correlation of 0, even though these signals are highly locked. PLV does not suffer from these drawbacks. Nonetheless, we have provided a direct comparison between PLV measures and Pearson correlation measures on the effect of measured anisotropy in the supplementary material (Fig. 2S). This shows that, for the current data under investigation, results are highly comparable. Given that the PLV measure is convenient to interpret (ie. are the signals phase locked), we opted to keep this measure.

We use the same frequency band (0.04–0.07 Hz) for RS and VFM. However, during VFM responses are locked to the stimuli period, the peak frequency band is lower than in RS. Generally in RS data, most power is below 0.03 Hz, however, the peak power might not be always the product of neuronal activity. Some scans can show peaks around 0.1 Hz or even higher. As shown by Glerean and colleagues, 0.04–0.07 Hz is the most reliable frequency band from which to extract resting state networks (Glerean et al., 2012). In VFM, we use the same frequency band as a in RS to be able to compare the results. We deliberately removed some of the possible useful information in the low frequency side because we are not pulling out the VFM response per-se but instead focus on spontaneous fluctuations and try to avoid contamination by low frequency artifacts (i.e. respiration).

The current study analyses stationary synchronization patterns only. As such, they provide a time averaged picture and do not capture potentially relevant transient dynamics (Liu and Duyn, 2013). Time-resolved methods such as the analysis of propagation and transient coactivation patterns might help disclose relevant dynamics such as visuotopically organized co-fluctuations, patterns of diffusion and possibly waves (Liu and Duyn, 2013; Matsui et al., 2016; Aquino et al., 2012). Further research is also required to establish the possible neuronal mechanisms underlying visuotopically organized covariations in the phase of fMRI signals. Adding independent measures of neurophysiological and visceral activity, like electroencephalography and electrogastrography, seems a promising path to study the relation of neuronal activity to hemostatic and visceral activity during resting state (Richter et al., 2017; Yuan et al., 2012). Future analyses could also take into account measures of blood flow, as blood arrival times are known to affect resting state functional connectivity (Erdoğan et al., 2016).

5. Conclusion

We have demonstrated that BOLD signals fluctuations across early visual cortical areas can be segmented into highly reproducible synchronization clusters irrespective whether they are derived from RS fMRI or visual field mapping data. Importantly, we show that the spatial footprint of these synchronization clusters is independent of the magnitude and spatial extent of PS in different RS and VFM scans and reflect the layout of homotopic anatomical connections along the visual hierarchy. This indicates that both intrinsic and stimulus-evoked fMRI fluctuations are anchored by the same neuroanatomical connections. The fact that the PS clusters for RS and VFM are similarly elongated in the eccentricity direction also points to a shared neuroanatomical basis. Our findings thus justify and facilitate direct comparison of RS and stimulus-evoked activity.

Acknowledgments

Nicolas Gravel was supported by the (Chilean) National Commission for Scientific and Technological Research (BECAS CHILE) and the Graduate School for Medical Sciences (GSMS) of the University Medical Center Groningen (UMCG). Ben M. Harvey, Remco J. Renken, Serge O. Dumoulin, and Frans W. Cornelissen were supported by the Netherlands Organization for Scientific Research (NWO Brain and Cognition grant 433-09-233). Ben Harvey as also supported by the Portuguese Foundation for Science and Technology grant #IF/01405/2014. We would like to thank Mathijs Raemaekers and colleagues for sharing their data.

Appendix A. Supplementary data

Supplementary data related to this article can be found at http://dx.doi.org/10.1016/j.neuroimage.2017.08.063.

References

Aquino, K.M., Schira, M.M., Robinson, P.A., Drysdale, P.M., Michael, B., 2012. Hemodynamic traveling waves in human visual cortex. PLoS Comput. Biol. 8 (3), e1002435.
Arcaro, M.J., Honey, C.J., Mruczek, R.E.B., Kastner, S., Hasson, U., 2015. Widespread correlation patterns of fMRI signal across visual cortex reflect eccentricity organization. Elife 4.
Betzel, R.F., Alessandra, G., Andrea, A.-K., Joaquín, G., Jean-Philippe, T., Patric, H., Olaf, S., 2013. Multi-scale community organization of the human structural connectome and its relationship with resting-state functional connectivity. Netw. Sci. 1 (03), 353–373.
Blondel, V.D., Guillaume, J.-L., Lambiotte, R., Lefebvre, E., 2008. Fast unfolding of communities in large networks. J. Stat. Mech. 2008 (10), P10008.
Blumenfeld, B., Bibitchkov, D., Tsodyks, M., 2006. Neural network model of the primary visual cortex: from functional architecture to lateral connectivity and back. J. Comput. Neurosci. 20 (2), 219–241.
Bock, A.S., Binda, P., Benson, N.C., Bridge, H., Watkins, K.E., Fine, I., 2015. Resting-State retinotopic organization in the absence of retinal input and visual experience. J. Neurosci. 35 (36), 12366–12382.
Bouma, H., 1970. Interaction effects in parafoveal letter recognition. Nature 226 (5241), 177–178.
Brainard, D.H., 1997. The psychophysics toolbox. Spat. Vis. 10 (4), 433–436.
Butt, O.H., Benson, N.C., Datta, R., Aguirre, G.K., 2013. The fine-scale functional correlation of striate cortex in sighted and blind people. J. Neurosci. 33 (41), 16209–16219.
Butt, O.H., Benson, N.C., Datta, R., Aguirre, G.K., 2015. Hierarchical and homotopic correlations of spontaneous neural activity within the visual cortex of the sighted and blind. Front. Hum. Neurosci. 9, 25.
Buzsáki, G., György, B., Kai, K., Marcus, R., 2007. Inhibition and brain work. Neuron 56 (5), 771–783.

Carandini, M., Shimaoka, D., Rossi, L.F., Sato, T.K., Benucci, A., Knöpfel, T., 2015. Imaging the awake visual cortex with a genetically encoded voltage indicator. J. Neurosci. 35 (1), 53–63.
Dijkstra, E.W., 1959. A note on two problems in connexion with graphs. Numer. Math. 1 (1), 269–271.
Dumoulin, S.O., Wandell, B.A., 2008. Population receptive field estimates in human visual cortex. Neuroimage 39 (2), 647–660.
Erdoğan, S.B., Tong, Y., Hocke, L.M., Lindsey, K.P., deB Frederick, B., 2016. Correcting for blood arrival time in global mean regression enhances functional connectivity analysis of resting state fMRI-BOLD signals. Front. Hum. Neurosci. 10, 311.
Formisano, E., Elia, F., Nikolaus, K., 2012. Seeing patterns through the hemodynamic veil — the future of pattern-information fMRI. Neuroimage 62 (2), 1249–1256.
Fox, M.D., 2010. Clinical applications of resting state functional connectivity. Front. Syst. Neurosci. 4 (19).
Glerean, E., Salmi, J., Lahnakoski, J.M., Jääskeläinen, I.P., Sams, M., 2012. Functional magnetic resonance imaging phase synchronization as a measure of dynamic functional connectivity. Brain Connect. 2 (2), 91–101.
Gravel, N., Harvey, B., Nordhjem, B., Haak, K.V., Dumoulin, S.O., Renken, R., Curčić-Blake, B., Cornelissen, F.W., 2014. Cortical connective field estimates from resting state fMRI activity. Front. Neurosci. 8, 339.
Haak, K.V., Winawer, J., Harvey, B.M., Renken, R., Dumoulin, S.O., Wandell, B.A., Cornelissen, F.W., 2013. Connective field modeling. Neuroimage 66, 376–384.
Hagler Jr., D.J., Saygin, A.P., Sereno, M.I., 2006. Smoothing and cluster thresholding for cortical surface-based group analysis of fMRI data. Neuroimage 33 (4), 1093–1103.
Harrison, R.V., Harel, N., Panesar, J., Mount, R.J., 2002. Blood capillary distribution correlates with hemodynamic-based functional imaging in cerebral cortex. Cereb. Cortex 12 (3), 225–233.
Harvey, B.M., Dumoulin, S.O., 2011. The relationship between cortical magnification factor and population receptive field size in human visual cortex: constancies in cortical architecture. J. Neurosci. 31 (38), 13604–13612.
Heinzle, J., Kahnt, T., Haynes, J.-D., 2011. Topographically specific functional connectivity between visual field maps in the human brain. Neuroimage 56 (3), 1426–1436.
Honey, C.J., Sporns, O., Cammoun, L., Gigandet, X., Thiran, J.P., Meuli, R., Hagmann, P., 2009. Predicting human resting-state functional connectivity from structural connectivity. Proc. Natl. Acad. Sci. U. S. A. 106 (6), 2035–2040.
Kamitani, Y., Tong, F., 2005. Decoding the visual and subjective contents of the human brain. Nat. Neurosci. 8 (5), 679–685.
Kastner, S., Pinsk, M.A., De Weerd, P., Desimone, R., Ungerleider, L.G., 1999. Increased activity in human visual cortex during directed attention in the absence of visual stimulation. Neuron 22 (4), 751–761.
Kenet, T., Bibitchkov, D., Tsodyks, M., Grinvald, A., Arieli, A., 2003. Spontaneously emerging cortical representations of visual attributes. Nature 425 (6961), 954–956.
Kooi, F.L., Toet, A., Tripathy, S.P., Levi, D.M., 1994. The effect of similarity and duration on spatial interaction in peripheral vision. Spat. Vis. 8 (2), 255–279.
Lachaux, J.P., Rodriguez, E., Martinerie, J., Varela, F.J., 1999. Measuring phase synchrony in brain signals. Hum. Brain Mapp. 8 (4), 194–208.
Lacy, T.C., Aquino, K.M., Robinson, P.A., Schira, M.M., 2016. Shock-like haemodynamic responses induced in the primary visual cortex by moving visual stimuli. J. R. Soc. Interface 13 (125).
Laird, A., Carew, J., Meyerand, M.E., 2001. Analysis of the instantaneous phase signal of a fMRI time series via the hilbert transform, Conference Record of Thirty-fifth Asilomar Conference on Signals, Systems and Computers (Cat.No.01CH37256).
Laird, A.R., Rogers, B.P., Carew, J.D., Arfanakis, K., Moritz, C.H., Meyerand, M.E., 2002. Characterizing instantaneous phase relationships in whole-brain fMRI activation data. Hum. Brain Mapp. 16 (2), 71–80.
Lee, A.T., Glover, G.H., Meyer, C.H., 1995. Discrimination of large venous vessels in time-course spiral blood-oxygen-level-dependent magnetic-resonance functional neuroimaging. Magn. Reson. Med. 33 (6), 745–754.
Lee, M.H., Smyser, C.D., Shimony, J.S., 2013. Resting-state fMRI: a review of methods and clinical applications. AJNR Am. J. Neuroradiol. 34 (10), 1866–1872.
Lewis, C.M., Bosman, C.A., Womelsdorf, T., Fries, P., 2016. Stimulus-induced visual cortical networks are recapitulated by spontaneous local and interareal synchronization. Proc. Natl. Acad. Sci. U. S. A. 113 (5), E606–E615.
Liu, X., Duyn, J.H., 2013. Time-varying functional network information extracted from brief instances of spontaneous brain activity. Proc. Natl. Acad. Sci. U. S. A. 110 (11), 4392–4397.
Logothetis, N.K., Pauls, J., Augath, M., Trinath, T., Oeltermann, A., 2001. Neurophysiological investigation of the basis of the fMRI signal. Nature 412 (6843), 150–157.
Logothetis, N.K., Wandell, B.A., 2004. Interpreting the BOLD signal. Annu. Rev. Physiol. 66, 735–769.
Logothetis, N.K., Yusuke, M., Mark, A., Theodor, S., Joachim, W., Axel, O., 2009. How not to study spontaneous activity. Neuroimage 45 (4), 1080–1089.
Matsui, T., Murakami, T., Ohki, K., 2016. Transient neuronal coactivations embedded in globally propagating waves underlie resting-state functional connectivity. Proc. Natl. Acad. Sci. U. S. A. 113 (23), 6556–6561.
Menon, R.S., Kim, S.G., 1999. Spatial and temporal limits in cognitive neuroimaging with fMRI. Trends Cogn. Sci. 3 (6), 207–216.
Nandy, A.S., Tjan, B.S., 2012. Saccade-confounded image statistics explain visual crowding. Nat. Neurosci. 15 (3), 463–469, S1–2.
Nestares, O., Heeger, D.J., 2000. Robust multiresolution alignment of MRI brain volumes. Magn. Reson. Med. 43 (5), 705–715.
OHerron, P., Philip, O., Chhatbar, P.Y., Manuel, L., Zhiming, S., Schramm, A.E., Zhongyang, K., Prakash, K., 2016. Neural correlates of single-vessel haemodynamic responses in vivo. Nature 534 (7607), 378–382.
Pang, J.C., Robinson, P.A., Aquino, K.M., Vasan, N., 2017. Effects of astrocytic dynamics on spatiotemporal hemodynamics: modeling and enhanced data analysis. Neuroimage 147, 994–1005.
Parker, A., Andrew, P., Holly, B., Gaelle, C., 2016. Spatial scale of correlated signals in 7T BOLD imaging, Proceedings of the 9th EAI International Conference on Bio-inspired Information and Communications Technologies (Formerly BIONETICS).
Pelli, D.G., 1997. The VideoToolbox software for visual psychophysics: transforming numbers into movies. Spat. Vis. 10 (4), 437–442.
Pelli, D.G., 2008. Crowding: a cortical constraint on object recognition. Curr. Opin. Neurobiol. 18 (4), 445–451.
Pisauro, M.A., Dhruv, N.T., Carandini, M., Benucci, A., 2013. Fast hemodynamic responses in the visual cortex of the awake mouse. J. Neurosci. 33 (46), 18343–18351.
Ponce-Alvarez, A., Deco, G., Hagmann, P., Romani, G.L., Mantini, D., Corbetta, M., 2015. Resting-state temporal synchronization networks emerge from connectivity topology and heterogeneity. PLoS Comput. Biol. 11 (2), e1004100.
Postnov, D.E., Sosnovtseva, O.V., Erik, M., 2005. Oscillator clustering in a resource distribution chain. Chaos An Interdiscip. J. Nonlinear Sci. 15 (1), 013704.
Raemaekers, M., Mathijs, R., Wouter, S., van Wezel, R.J.A., Natalia, P., Gert, K., Ramsey, N.F., 2014. Patterns of resting state connectivity in human primary visual cortical areas: a 7T fMRI study. Neuroimage 84, 911–921.
Raichle, M.E., 2015. The restless brain: how intrinsic activity organizes brain function. Philos. Trans. R. Soc. Lond. B Biol. Sci. 370 (1668), 20140172.
Ramot, M., Wilf, M., Goldberg, H., Weiss, T., Deouell, L.Y., Malach, R., 2011. Coupling between spontaneous (resting state) fMRI fluctuations and human oculo-motor activity. Neuroimage 58 (1), 213–225.
Richter, C.G., Babo-Rebelo, M., Schwartz, D., Tallon-Baudry, C., 2017. Phase-amplitude coupling at the organism level: the amplitude of spontaneous alpha rhythm fluctuations varies with the phase of the infra-slow gastric basal rhythm. Neuroimage 146, 951–958.
Roseman, L., Sereno, M.I., Leech, R., Kaelen, M., Orban, C., McGonigle, J., Feilding, A., Nutt, D.J., Carhart-Harris, R.L., 2016. LSD alters eyes-closed functional connectivity within the early visual cortex in a retinotopic fashion. Hum. Brain Mapp. 37 (8), 3031–3040.
Rubinov, M., Sporns, O., 2010. Complex network measures of brain connectivity: uses and interpretations. Neuroimage 52 (3), 1059–1069.
Schellekens, W., Van Wezel, R.J.A., Petridou, N., Ramsey, N.F., Raemaekers, M., 2013. Integration of motion responses underlying directional motion anisotropy in human early visual cortical areas. PLoS One 8 (6), e67468.
Schira, M.M., Tyler, C.W., Breakspear, M., Spehar, B., 2009. The foveal confluence in human visual cortex. J. Neurosci. 29 (28), 9050–9058.
Schira, M.M., Tyler, C.W., Spehar, B., Breakspear, M., 2010. Modeling magnification and anisotropy in the primate foveal confluence. PLoS Comput. Biol. 6 (1), e1000651.
Tass, P., Rosenblum, M.G., Weule, J., Kurths, J., Pikovsky, A., Volkmann, J., Schnitzler, A., Freund, H.-J., 1998. Detection of n : m phase locking from noisy data: application to magnetoencephalography. Phys. Rev. Lett. 81 (15), 3291–3294.
Teo, P.C., Sapiro, G., Wandell, B.A., 1997. Creating connected representations of cortical gray matter for functional MRI visualization. IEEE Trans. Med. Imaging 16 (6), 852–863.
Toet, A., Levi, D.M., 1992. The two-dimensional shape of spatial interaction zones in the parafovea. Vis. Res. 32 (7), 1349–1357.
Tong, Y., Hocke, L.M., Fan, X., Janes, A.C., Frederick, B.D., 2015. Can apparent resting state connectivity arise from systemic fluctuations? Front. Hum. Neurosci. 9, 285.
Tong, Y., Yunjie, T., Hocke, L.M., Lindsey, K.P., Erdoğan, S.B., Gordana, V., Caine, C.E., Frederick, B.D., 2016. Systemic Low-Frequency oscillations in BOLD signal vary with tissue type. Front. Neurosci. 10.
Tsodyks, M., Kenet, T., Grinvald, A., Arieli, A., 1999. Linking spontaneous activity of single cortical neurons and the underlying functional architecture. Science 286 (5446), 1943–1946.
van den Berg, R., Johnson, A., Martinez Anton, A., Schepers, A.L., Cornelissen, F.W., 2012. Comparing crowding in human and ideal observers. J. Vis. 12 (6), 13.
Vazquez, A.L., Murphy, M.C., Kim, S.-G., 2014. Neuronal and physiological correlation to hemodynamic resting-state fluctuations in health and disease. Brain Connect. 4 (9), 727–740.
Vincent, J.L., Patel, G.H., Fox, M.D., Snyder, A.Z., Baker, J.T., Van Essen, D.C., Zempel, J. M., Snyder, L.H., Corbetta, M., Raichle, M.E., 2007. Intrinsic functional architecture in the anaesthetized monkey brain. Nature 447 (7140), 83–86.
Vinck, M., Bosman, C.A., 2016. More gamma more predictions: gamma-Synchronization as a key mechanism for efficient integration of classical receptive field inputs with surround predictions. Front. Syst. Neurosci. 10, 35.
Wandell, B.A., Chial, S., Backus, B.T., 2000. Visualization and measurement of the cortical surface. J. Cogn. Neurosci. 12 (5), 739–752.
Winawer, J., Horiguchi, H., Sayres, R.A., Amano, K., Wandell, B.A., 2010. Mapping hv4 and ventral occipital cortex: the venous eclipse. J. Vis. 10 (5), 1.
Ye, J., Lazar, N.A., Li, Y., 2015. Nonparametric variogram modeling with hole effect structure in analyzing the spatial characteristics of fMRI data. J. Neurosci. Methods 240, 101–115.
Yeo, B.T.T., Krienen, F.M., Sepulcre, J., Sabuncu, M.R., Lashkari, D., Hollinshead, M., Roffman, J.L., Smoller, J.W., Zöllei, L., Polimeni, J.R., Fischl, B., Liu, H., Buckner, R. L., 2011. The organization of the human cerebral cortex estimated by intrinsic functional connectivity. J. Neurophysiol. 106 (3), 1125–1165.
Yuan, H., Han, Y., Vadim, Z., Raquel, P., Drevets, W.C., Jerzy, B., 2012. Spatiotemporal dynamics of the brain at rest — exploring EEG microstates as electrophysiological signatures of BOLD resting state networks. Neuroimage 60 (4), 2062–2072.